Published in Geomechanics for Energy and the Environment, 2015, 4, 29-38;
doi:10.1016/j.gete.2015.09.001

Elastoplastic coupling for thermo-elasto-plasticity at high temperature

Alessandro Gajo, Davide Bigoni

Dipartimento di Ingegneria Civile, Ambientale e Meccanica,
Università di Trento, Via Mesiano 77, I-38123 Trento, Italia

Dedicated to Prof. Tomasz Hueckel, on the occasion of his 70th birthday.

Abstract

The coupling of elastic and plastic deformation is introduced in a framework allowing for the inclusion of thermal effects. In this context where high temperatures may be present, many laws governing materials behaviour become nonlinear functions of both temperature and strain. The understanding of this is crucial to the modelling the behavoiur of refractories, sintering processes, rocks at great depth and geo-energy. Two equivalent formulations are presented, one in terms of isothermal elastic quantities and the other in terms of adiabatic. In the former approach a Helmoltz free energy density need not be introduced and the contributions to the variations of elastic stiffness of both plastic flow and temperature can be clearly separated and hence a full explanation given. A simple example using available experiments on sintered alumina shows the capability of the constitutive framework to describe the behaviour of refractories at high temperature.

Keywords: Elasticity, plasticity, flow rule

1 Introduction

Refractories for applications in the liquid steel industry [8], ceramic powders subject to sintering [22, 10], rocks in the earth's mantle or for heat involved in heat storage or geothermal-energy exploitation at great depth [11], and concrete for fire protection [20] are all examples of materials working under extreme temperature environments or

[1]Corresponding author: Davide Bigoni - fax: +39 0461 882599; tel.: +39 0461 882507; website: http://www.ing.unitn.it/∼bigoni/; e-mail: bigoni@ing.unitn.it.

subject to high temperature excursions. In all these cases plastic flow which is caused by sliding between grains, nucleation and growth of pores and microcracks affects the elastic properties of the materials. These phenomena can be modelled using the concept of elastoplastic coupling, a concept that was pioneered and developed by Tomasz Huekel [16, 17, 18, 21, 4], to whom this article is dedicated. In the above-mentioned materials, temperature is known to influence yielding, hardening, and elasticity, but it may have antagonistic effects on damage, so that, while a thermal shock can microfracture a brittle material, adhesion between particles occurs during sintering and an analogous phenomenon of microfracture healing may happen as a consequence of local melting at crack surfaces in fissured rock.

Research on elastoplastic coupling has developed to include multisurface effects [5], models for the densification processes of granulates [23],[24], [25], [26] and models for the mechanical response of sand [12]. This has proved to be of crucial importance in capturing strain localization in granular media under drained conditions [14], [15]. An important step forward in this activity was the realization that assuming normality for the rate of irreversible strain (rather than of plastic strain) to the yield surface implies that the constitutive operator is symmetric [14], an observation which becomes crucial in the definition of maximum dissipation.

The present article is focused on a class of materials displaying only reversible strain when subjected to thermal load/unload cycles, with the stress state lying within the yield surface. This reversibility is typical of single-constituent refractory materials (such as sintered alumina [28, 9]) and implies that a temperature variation may produce plastic strain only if the stress state lies on the yield surface. This behaviour is in contrast with materials (made up with various constituents of different thermal expansion coefficients [19]) displaying irreversible strains when subjected to thermal load/unload cycles at null applied stresses, thus involving a complex coupling between plastic strain and temperature. The purpose of the present article is to develop the formulation of elastoplastic coupling for the modelling of thermoplastic behaviour of rock-like and refractory materials. The main complication here arises from the fact that several constitutive laws, usually assumed to be linear, become nonlinear for high temperature excursions and functions of both plastic strain (which measures the damage of the material) and temperature. Therefore, following [2], the formulation will first be introduced as a direct extension of elastoplastic coupling under isothermal conditions (Section 2.1), which does not require the introduction of a free energy density function, and later transformed in to an adiabatic form (Section 2.2). The treatment is done in such a way that the contributions of elastoplastic coupling and of temperature on variation of elastic stiffness are clearly separated. This separation is crucial to describe the sometimes contrasting effects of damage (reducing the elastic stiffness) and temperature (which, when extreme, may induce melting and damage healing). Finally, an application is presented to describe the sintering of a ceramic powder or refractory material in which the self-healing occurs with exposure to high temperature. (Section 3). The example is calibrated using data exper-

iments with sintered alumina and shows the capability of the constitutive framework for the description of rock-like materials at high temperature.

2 Thermoplastic constitutive equations

Two formulations are introduced for thermo-elasto-plastic constitutive equations in which the plastic deformation influences the elastic response of the material ('elastoplastic coupling'), with a full account of all couplings related to the temperature effects. The first formulation, obtained as a direct extension of the elastoplastic coupling concept under isothermal conditions, does not require the introduction of a Helmholtz free energy density, while the second formulation does require its introduction, based on adiabatic quantities.

2.1 Formulation in isothermal form

The strain $\boldsymbol{\epsilon}$ is additively decomposed into the elastic (subscript 'e'), plastic (subscript 'p'), and thermal (subscript 'T') parts as

$$\boldsymbol{\epsilon} = \boldsymbol{\epsilon}_e + \boldsymbol{\epsilon}_p + \boldsymbol{\epsilon}_T, \tag{1}$$

where the thermal strain $\boldsymbol{\epsilon}_T$ can be a complicated tensorial function of the temperature variation ΔT. In the case of isotropic response, the thermal strain is equal to

$$\boldsymbol{\epsilon}_T = \alpha_{(T)} \Delta T \, \mathbf{I}. \tag{2}$$

where the thermal expansion coefficient $\alpha_{(T)}$ can be constant or assumed to be a function of the temperature.

The stress can be expressed as a function of the strain, of its plastic part, and of the temperature

$$\boldsymbol{\sigma} = \boldsymbol{\sigma}\left(\boldsymbol{\epsilon}, \boldsymbol{\epsilon}_p, T\right), \tag{3}$$

implying a precise choice of independent variables. For instance, the stress can be a linear relation of the elastic strain through a fourth-order elastic tensor $\mathbb{E}_i$, which may depend on both temperature and plastic strain, namely, $\mathbb{E}_i(\boldsymbol{\epsilon}_p, T)$, so that

$$\boldsymbol{\sigma} = \mathbb{E}_{i\,(\boldsymbol{\epsilon}_p, T)}[\boldsymbol{\epsilon} - \boldsymbol{\epsilon}_p] + \Delta T \mathbf{C}_{(\boldsymbol{\epsilon}_p, T)}. \tag{4}$$

The subscript '$(\boldsymbol{\epsilon}_p, T)$' highlights the functional dependence of the quantity on the plastic strain and the temperature. In equation (4), $\mathbf{C}$ is a second-order symmetric tensor, that, in the particular case of isotropic thermal strain and isotropic elastic bulk response, reduces to

$$\Delta T \mathbf{C}_{(\boldsymbol{\epsilon}_p, T)} = -\mathbb{E}_{i\,(\boldsymbol{\epsilon}_p, T)}[\boldsymbol{\epsilon}_T] = -3K_{i\,(\boldsymbol{\epsilon}_p, T)} \alpha_{(T)} \Delta T \, \mathbf{I}, \tag{5}$$

where $K_{i\,(\boldsymbol{\epsilon}_p,T)}$ is the elastic isothermal bulk modulus, which may be function of both the plastic strain and the temperature, $K_i(\boldsymbol{\epsilon}_p, T)$.

The stress-temperature tensor is defined as

$$\mathbf{B} = \frac{\partial \boldsymbol{\sigma}(\boldsymbol{\epsilon}, \boldsymbol{\epsilon}_p, T)}{\partial T}, \tag{6}$$

so that, accepting representation (4) becomes

$$\mathbf{B} = \frac{\partial \mathbb{E}_{i\,(\boldsymbol{\epsilon}_p,T)}}{\partial T}[\boldsymbol{\epsilon} - \boldsymbol{\epsilon}_p] + \Delta T \frac{\partial \mathbf{C}_{(\boldsymbol{\epsilon}_p,T)}}{\partial T} + \mathbf{C}_{(\boldsymbol{\epsilon}_p,T)}. \tag{7}$$

It can be noted that, for the simplified law (5), the derivative of $\mathbf{C}$ with respect to the temperature reduces to

$$\Delta T \frac{\partial \mathbf{C}_{(\boldsymbol{\epsilon}_p,T)}}{\partial T} = -3\Delta T \frac{\partial K_{i\,(\boldsymbol{\epsilon}_p,T)}}{\partial T} \alpha_{(T)}\,\mathbf{I} - 3\Delta T K_{i\,(\boldsymbol{\epsilon}_p,T)} \frac{\partial \alpha_{(T)}}{\partial T}\,\mathbf{I}, \tag{8}$$

which, for constant $\alpha_{(T)}$, is only a measure of the temperature variation of the elastic stiffness.

Taking the derivative of equation (4) with respect to the time, and accepting elasto-plastic coupling (so that the dependence of $\mathbb{E}_{i\,(\boldsymbol{\epsilon}_p,T)}$ on the plastic strain is not neglected), the stress rate can be expressed as

$$\dot{\boldsymbol{\sigma}} = \frac{\partial \boldsymbol{\sigma}}{\partial \boldsymbol{\epsilon}}[\dot{\boldsymbol{\epsilon}}] + \frac{\partial \boldsymbol{\sigma}}{\partial \boldsymbol{\epsilon}_p}[\dot{\boldsymbol{\epsilon}}_p] + \mathbf{B}\,\dot{T}, \tag{9}$$

from which the elastoplastic coupling can be given evidence as

$$\dot{\boldsymbol{\sigma}} = \frac{\partial \boldsymbol{\sigma}}{\partial \boldsymbol{\epsilon}}[\dot{\boldsymbol{\epsilon}} - \dot{\boldsymbol{\epsilon}}_p] + \underbrace{\left(\frac{\partial \boldsymbol{\sigma}}{\partial \boldsymbol{\epsilon}_p} + \frac{\partial \boldsymbol{\sigma}}{\partial \boldsymbol{\epsilon}}\right)[\dot{\boldsymbol{\epsilon}}_p]}_{elastoplastic\ coupling} + \mathbf{B}\,\dot{T}. \tag{10}$$

Accepting representation (4), the stress rate can be expressed as

$$\dot{\boldsymbol{\sigma}} = \mathbb{E}_{i\,(\boldsymbol{\epsilon}_p,T)}[\dot{\boldsymbol{\epsilon}}] - \left(\mathbb{E}_{i\,(\boldsymbol{\epsilon}_p,T)} \underbrace{- \frac{\partial \mathbb{E}_{i\,(\boldsymbol{\epsilon}_p,T)}}{\partial \boldsymbol{\epsilon}_p}[\boldsymbol{\epsilon} - \boldsymbol{\epsilon}_p] - \Delta T \frac{\partial \mathbf{C}_{(\boldsymbol{\epsilon}_p,T)}}{\partial \boldsymbol{\epsilon}_p}}_{elastoplastic\ coupling}\right)[\dot{\boldsymbol{\epsilon}}_p] + \mathbf{B}\,\dot{T}. \tag{11}$$

Equations (7) and (11) clearly separate the plastic dependence from the temperature dependence of the elastic stiffness, the former representing the elastoplastic coupling.

The irreversible strain rate $\dot{\boldsymbol{\epsilon}}_i$ is defined as

$$\dot{\boldsymbol{\epsilon}}_i = \mathbb{C}[\dot{\boldsymbol{\epsilon}}_p], \tag{12}$$

where the fourth-order tensor

$$\mathbb{C} = \mathbb{S} - \mathbb{E}^{-1}_{i\,(\boldsymbol{\epsilon}_p,T)} \left(\frac{\partial \mathbb{E}_{i\,(\boldsymbol{\epsilon}_p,T)}}{\partial \boldsymbol{\epsilon}_p}[\boldsymbol{\epsilon} - \boldsymbol{\epsilon}_p] + \Delta T \frac{\partial \mathbf{C}_{(\boldsymbol{\epsilon}_p,T)}}{\partial \boldsymbol{\epsilon}_p} \right), \tag{13}$$

in which $\mathbb{S}$ is the fourth-order symmetrizer, is assumed to be invertible. The rate equation (10) can be rewritten as

$$\dot{\boldsymbol{\sigma}} = \mathbb{E}_{i\,(\boldsymbol{\epsilon}_p,T)}[\dot{\boldsymbol{\epsilon}}] - \mathbb{E}_{i\,(\boldsymbol{\epsilon}_p,T)}[\dot{\boldsymbol{\epsilon}}_i] + \dot{T}\mathbf{B}. \tag{14}$$

Rather than the rate of plastic strain, the plastic flow rule is assumed to govern the rate of the inelastic strain, so that

$$\dot{\boldsymbol{\epsilon}}_i = \dot{\lambda}\mathbf{P}(\boldsymbol{\sigma}, \boldsymbol{\epsilon}_p, T), \tag{15}$$

where $\dot{\lambda} \geq 0$ is the plastic multiplier and $\mathbf{P}$ the plastic flow mode tensor, a function of the stress, of the plastic strain and of the temperature. Tensor $\mathbf{P}$ is not in general normal to the yield surface, so that the flow rule (15) is for the moment assumed nonassociative. The normality rule corresponds in the present context to the condition for which $\dot{\boldsymbol{\epsilon}}_i$ and the yield function gradient are coaxial. The reasons to assume that the flow flows rule (15) determines the 'direction' of the rate of inelastic deformation, instead than the rate of plastic strain, have been explained in detail in [14] and are consistent with concepts introduced by Collins & Houlsby (1997), based on Ziegler's orthogonality principle (1983). A substitution of equation (15) in equation (14) yields

$$\dot{\boldsymbol{\sigma}} = \mathbb{E}_{i\,(\boldsymbol{\epsilon}_p,T)}[\dot{\boldsymbol{\epsilon}}] - \dot{\lambda}\mathbb{E}_{i\,(\boldsymbol{\epsilon}_p,T)}[\mathbf{P}] + \dot{T}\mathbf{B}. \tag{16}$$

Note that

$$\dot{\boldsymbol{\epsilon}}_p = \dot{\lambda}\mathbb{C}^{-1}[\mathbf{P}], \tag{17}$$

so that when $\dot{\lambda} = 0$ both $\dot{\boldsymbol{\epsilon}}_p$ and $\dot{\boldsymbol{\epsilon}}_i$ vanish simultaneously.

The yield function is assumed in the form

$$f = f(\boldsymbol{\sigma}, \mathcal{H}, T), \tag{18}$$

where $\mathcal{H}$ denotes a collection of generic hardening parameters, now functions of the temperature T and, as usual, of the plastic deformation $\boldsymbol{\epsilon}_p$. The yield function gradient is denoted by

$$\mathbf{Q} = \frac{\partial f}{\partial \boldsymbol{\sigma}}, \tag{19}$$

so that the Prager's consistency can be written as

$$\dot{f} = \mathbf{Q} \cdot \dot{\boldsymbol{\sigma}} + \frac{\partial f}{\partial \mathcal{H}} \cdot \dot{\mathcal{H}} + \frac{\partial f}{\partial T} \cdot \dot{T} = 0, \tag{20}$$

when plastic loading occurs.

Introducing now the hardening modulus h_i as

$$\dot{\lambda} h_i = -\frac{\partial f}{\partial \mathcal{H}} \dot{\mathcal{H}}, \tag{21}$$

and the (strictly positive) plastic modulus

$$H_i = \mathbf{Q} \cdot \mathbb{E}_{i\,(\boldsymbol{\epsilon}_p, T)}[\mathbf{P}] + h_i, \tag{22}$$

the plastic multiplier can be derived from a substitution of equation (16) into the consistency equation (20)

$$\dot{\lambda} = \frac{< \mathbf{Q} \cdot \mathbb{E}_{i\,(\boldsymbol{\epsilon}_p, T)}[\dot{\boldsymbol{\epsilon}}] + \left(\mathbf{B} \cdot \mathbf{Q} + \dfrac{\partial f}{\partial T} \right) \dot{T} >}{H_i}, \tag{23}$$

where $<>$ are the Macaulay brackets, enforcing the distinction between plastic loading, elastic unloading, and neutral loading.

A substitution of equation (23) into equation (16) yields the thermo-elasto-plastic constitutive equations in the following rate form involving isothermal elastic moduli

$$\dot{\boldsymbol{\sigma}} = \mathbb{E}_{i\,(\boldsymbol{\epsilon}_p, T)}[\dot{\boldsymbol{\epsilon}}] - \frac{< \mathbf{Q} \cdot \mathbb{E}_{i\,(\boldsymbol{\epsilon}_p, T)}[\dot{\boldsymbol{\epsilon}}] - \beta \dot{T} >}{\mathbf{Q} \cdot \mathbb{E}_{i\,(\boldsymbol{\epsilon}_p, T)}[\mathbf{P}] + h_i} \mathbb{E}_{i\,(\boldsymbol{\epsilon}_p, T)}[\mathbf{P}] + \dot{T} \mathbf{B}, \tag{24}$$

where

$$\beta = -\mathbf{B} \cdot \mathbf{Q} - \frac{\partial f}{\partial T}. \tag{25}$$

Note that the normality rule corresponds to the special case in which $\mathbf{P} = \mathbf{Q}$.

2.2 Formulation in adiabatic form

In order to express the rate constitutive equations (24) in an adiabatic form, the Helmholtz free energy density per unit mass has to be introduced

$$\psi = \psi(\boldsymbol{\epsilon}, \boldsymbol{\epsilon}_p, T), \tag{26}$$

which is consistent with the choice of the independent variables in equation (4) and is related to the specific internal energy e and the specific entropy s through

$$\psi = e - Ts, \tag{27}$$

and defined so that

$$\boldsymbol{\sigma} = \rho \frac{\partial \psi}{\partial \boldsymbol{\epsilon}}, \quad s = -\frac{\partial \psi}{\partial T}. \tag{28}$$

Local conservation of energy or the First Law of Thermodynamics is (Truesdell and Toupin, 1960)

$$\rho\dot{e} = \boldsymbol{\sigma}\cdot\dot{\boldsymbol{\epsilon}} - \mathrm{div}\mathbf{q} + r, \tag{29}$$

where r is the heat supply per unit volume generated by internal sources, $\mathbf{q}$ is the heat flux, assumed to obey a generalized Fourier law of heat conduction

$$\mathbf{q} = -\mathbf{K}\,\nabla T, \tag{30}$$

in which tensor $\mathbf{K}$ may be a generic function of the state varables (for instance plastic strain and temperature), but is always positive definite. Local adiabatic conditions correspond to $r = \mathrm{div}\mathbf{q} = 0$.

With a slight loss of generality, but a considerable gain in simplicity, the Helmholtz free energy per unit mass can be expressed in a convenient form as

$$\psi(\boldsymbol{\epsilon},\boldsymbol{\epsilon}_p,T) = \frac{1}{2\rho}(\boldsymbol{\epsilon}-\boldsymbol{\epsilon}_p)\cdot\mathbb{E}_{i\,(\boldsymbol{\epsilon}_p,T)}[\boldsymbol{\epsilon}-\boldsymbol{\epsilon}_p] + \frac{\Delta T}{\rho}\mathbf{C}_{(\boldsymbol{\epsilon}_p,T)}\cdot(\boldsymbol{\epsilon}-\boldsymbol{\epsilon}_p) - \tilde{c}_{v\,(\boldsymbol{\epsilon}_p,T)}\left(T\log\frac{T}{T_0} - \Delta T\right), \tag{31}$$

where again the subscript '$(\boldsymbol{\epsilon}_p,T)$' highlights the functional dependence of the quantity on the plastic strain and the temperature, T_0 is a reference temperature, and $\tilde{c}_{v\,(\boldsymbol{\epsilon}_p,T)}$ is a function of the plastic strain and of the temperature, which may describe the temperature dependence of heat capacity.

The Helmoltz free energy (31) leads through equation $(28)_1$ to exactly the same expression (4) for the stress, while equation $(28)_2$ yields

$$\begin{aligned} s \;&= -\frac{1}{2\rho}(\boldsymbol{\epsilon}-\boldsymbol{\epsilon}_p)\cdot\frac{\partial\mathbb{E}_{i\,(\boldsymbol{\epsilon}_p,T)}}{\partial T}[\boldsymbol{\epsilon}-\boldsymbol{\epsilon}_p] - \frac{1}{\rho}\mathbf{C}_{(\boldsymbol{\epsilon}_p,T)}\cdot(\boldsymbol{\epsilon}-\boldsymbol{\epsilon}_p) \\ &\quad -\frac{\Delta T}{\rho}\frac{\partial\mathbf{C}_{(\boldsymbol{\epsilon}_p,T)}}{\partial T}\cdot(\boldsymbol{\epsilon}-\boldsymbol{\epsilon}_p) + \tilde{c}_{v\,(\boldsymbol{\epsilon}_p,T)}\log\frac{T}{T_0} + \frac{\partial\tilde{c}_{v\,(\boldsymbol{\epsilon}_p,T)}}{\partial T}\left(T\log\frac{T}{T_0} - \Delta T\right). \end{aligned} \tag{32}$$

Note that, when $\mathbb{E}_i$ and $\mathbf{C}$ are independent of the temperature, tensor $\mathbf{C}$ coincides with the stress-temperature tensor, $\mathbf{B} = \mathbf{C}$, and $\tilde{c}_{v\,(\boldsymbol{\epsilon}_p,T)}$ becomes the specific heat at constant strain.

Taking the time derivative of the Helmholtz free energy (26) and using equations (28) and (29) yields

$$\dot{e} = \boldsymbol{\sigma}\cdot\dot{\boldsymbol{\epsilon}} + \frac{\partial\psi}{\partial\boldsymbol{\epsilon}_p}\cdot\dot{\boldsymbol{\epsilon}}_p + T\dot{s} \tag{33}$$

and

$$T\dot{s} = -\frac{\partial\psi}{\partial\boldsymbol{\epsilon}_p}\cdot\dot{\boldsymbol{\epsilon}}_p + \frac{\gamma}{\rho}, \tag{34}$$

where $\gamma = -\mathrm{div}\mathbf{q} + r$. The rate of the specific entropy is

$$\dot{s} = -\left(\frac{\partial\psi}{\partial T}\right)^{\cdot} = -\frac{\partial^2\psi}{\partial\boldsymbol{\epsilon}\partial T}\cdot\dot{\boldsymbol{\epsilon}} - \frac{\partial^2\psi}{\partial\boldsymbol{\epsilon}_p\partial T}\cdot\dot{\boldsymbol{\epsilon}}_p - \frac{\partial^2\psi}{\partial T^2}\dot{T}, \tag{35}$$

which, used in equation (34), leads to

$$\rho c_v \dot{T} = T\mathbf{B} \cdot \dot{\boldsymbol{\epsilon}} + \rho \left(T \frac{\partial^2 \psi}{\partial \boldsymbol{\epsilon}_p \partial T} - \frac{\partial \psi}{\partial \boldsymbol{\epsilon}_p} \right) \cdot \dot{\boldsymbol{\epsilon}}_p + \gamma. \tag{36}$$

where

$$c_v = -T \frac{\partial^2 \psi}{\partial T^2} \tag{37}$$

is the heat capacity at constant strain.

In the case of elastoplastic coupling, equation (17), used into equation (36), provides

$$\rho c_v \dot{T} = T\mathbf{B} \cdot \dot{\boldsymbol{\epsilon}} + \dot{\lambda}\rho \left(T \frac{\partial^2 \psi}{\partial \boldsymbol{\epsilon}_p \partial T} - \frac{\partial \psi}{\partial \boldsymbol{\epsilon}_p} \right) \cdot \mathbb{C}^{-1}[\mathbf{P}] + \gamma. \tag{38}$$

Therefore, by introducing

$$\chi = \rho \left(\frac{\partial^2 \psi}{\partial \boldsymbol{\epsilon}_p \partial T} - \frac{1}{T} \frac{\partial \psi}{\partial \boldsymbol{\epsilon}_p} \right) \cdot \mathbb{C}^{-1}[\mathbf{P}], \tag{39}$$

which, using equation (31), can be specified to be

$$\begin{aligned} \rho \frac{\partial \psi}{\partial \boldsymbol{\epsilon}_p} &= -\boldsymbol{\sigma} + \frac{1}{2}(\boldsymbol{\epsilon} - \boldsymbol{\epsilon}_p) \cdot \frac{\partial \mathbb{E}_{i\,(\boldsymbol{\epsilon}_p, T)}}{\partial \boldsymbol{\epsilon}_p}[\boldsymbol{\epsilon} - \boldsymbol{\epsilon}_p] + \Delta T \left(\frac{\partial \mathbf{C}}{\partial \boldsymbol{\epsilon}_p} \right)^T [\boldsymbol{\epsilon} - \boldsymbol{\epsilon}_p], \\ \rho \frac{\partial^2 \psi}{\partial \boldsymbol{\epsilon}_p \partial T} &= -\mathbf{B} + \left(\frac{\partial \mathbf{C}}{\partial \boldsymbol{\epsilon}_p \partial T} + \Delta T \frac{\partial^2 \mathbf{C}}{\partial \boldsymbol{\epsilon}_p \partial T} \right)^T [\boldsymbol{\epsilon} - \boldsymbol{\epsilon}_p], \end{aligned} \tag{40}$$

two equations allowing to rewrite equation (36) as

$$\rho c_v \dot{T} = T\mathbf{B} \cdot \dot{\boldsymbol{\epsilon}} + \dot{\lambda} T \chi + \gamma. \tag{41}$$

Setting the elastoplastic coupling to be zero

$$\rho \frac{\partial \psi}{\partial \boldsymbol{\epsilon}_p} = -\boldsymbol{\sigma}, \quad \rho \frac{\partial^2 \psi}{\partial \boldsymbol{\epsilon}_p \partial T} = -\frac{\partial \boldsymbol{\sigma}}{\partial T} = -\mathbf{B}, \quad \mathbb{C}^{-1}[\mathbf{P}] = \mathbf{P}, \tag{42}$$

the following equation is immediately obtained

$$\chi = -\left(\mathbf{B} - \boldsymbol{\sigma}\right) \cdot \mathbf{P}, \tag{43}$$

so that $\chi \neq \beta$ even when $\mathbf{P} = \mathbf{Q}$.

The rate constitutive equations (24) can be expressed with adiabatic elastic stiffness, so that the plastic multiplier (23) can be rewritten using equation (41) as

$$\dot{\lambda} = \frac{< \mathbf{N}_a \cdot \dot{\boldsymbol{\epsilon}} - \dfrac{\beta \gamma}{\rho c_v} >}{H_i + \dfrac{T \beta \chi}{\rho c_v}} \tag{44}$$

and the stress rate as

$$\dot{\boldsymbol{\sigma}} = \mathbb{E}_a[\dot{\boldsymbol{\epsilon}}] - \dot{\lambda}\mathbf{M}_a + \frac{\gamma}{\rho c_v}\mathbf{B}, \tag{45}$$

where

$$\mathbb{E}_a = \mathbb{E}_{i\,(\boldsymbol{\epsilon}_p,T)} + \frac{T}{\rho c_v}\mathbf{B}\otimes\mathbf{B}, \tag{46}$$

is the adiabatic elastic fourth-order tensor and

$$\mathbf{M}_a = \mathbb{E}_{i\,(\boldsymbol{\epsilon}_p,T)}[\mathbf{P}] - \frac{T\chi}{\rho c_v}\mathbf{B}, \quad \mathbf{N}_a = \mathbb{E}^T_{i\,(\boldsymbol{\epsilon}_p,T)}\mathbf{Q} - \frac{T\beta}{\rho c_v}\mathbf{B}. \tag{47}$$

Therefore, the rate constitutive equations expressed in an adiabatic form are obtained as

$$\dot{\boldsymbol{\sigma}} = \mathbb{E}_a[\dot{\boldsymbol{\epsilon}}] - \frac{< \mathbf{N}_a \cdot \dot{\boldsymbol{\epsilon}} - \dfrac{\beta\gamma}{\rho c_v} >}{H_i + \dfrac{T\beta\chi}{\rho c_v}}\mathbf{M}_a + \frac{\gamma}{\rho c_v}\mathbf{B}. \tag{48}$$

Note that, due to the difference between β and χ, tensor $\mathbf{M}_a$ differs from tensor $\mathbf{N}_a$, so that the major symmetry of the constitutive operator is lost even when the normality rule applies, namely, when $\mathbf{P} = \mathbf{Q}$.

3 Specialization of the constitutive framework to the simulation of the thermomechanical behaviour of sintered alumina

In order to show the capabilities of the proposed thermo-elasto-plastic framework with elastoplastic coupling, a simple application is presented, which is calibrated using experimental results available on sintered alumina, using the interpolating relationships proposed by Gajo and Cecinato [13] and the compaction pressure vs. plastic volumetric strain law provided by Cooper and Eaton [7]. Moreover, the thermal softening of the material is assumed to follow the same tendency observed for the elastic modulus, whereas the mechanical softening and the damage of elastic stiffness due to shear loading are assumed to follow a reasonably expected trend. Note that softening can yield localized deformation, which is however not addressed here for simplicity. A rigorous analysis of localization and post-localization regime of a laboratory sample can be found in [14]. The simulations presented below show that the proposed constitutive framework may find application in the analysis of hot sintering under isostatic pressure (in other words, 'hot compaction') and in the simulation of refractory and rock response at high temperatures under severe mechanical isotropic and shear loadings. The simplifications introduced in the modelling imply that the gain in cohesion induced by firing (that is a factor even at null applied isostatic stress) is not captured for hot sintering, even if this effect could be easily introduced, if the experimental data were available.

3.1 Free energy density and elasto-plastic coupling

Experimental evidence on sintered alumina subjected to a thermal loading-unloading cycle ([9], [28]) suggests the assumption of the following free energy density function (expressed per unit mass, assumed equal to 3950 Kg/m^3)

$$\psi(\boldsymbol{\epsilon}, \boldsymbol{\epsilon}_p, T) = \frac{1}{2\,\rho} K_{i\,(\boldsymbol{\epsilon}_p,T)} \left[\mathrm{tr}(\boldsymbol{\epsilon} - \boldsymbol{\epsilon}_p) - \alpha_{(T)} \Delta T\right]^2 + \frac{G_{i\,(\boldsymbol{\epsilon}_p,T)}}{\rho} \left(\mathbf{e} - \mathbf{e}_p\right) \cdot \left(\mathbf{e} - \mathbf{e}_p\right) +$$

$$- \tilde{c}_{p\,(T)} \left(T \log\left(\frac{T}{T_0}\right) - \Delta T \right), \tag{49}$$

where $\mathbf{e}$ is the deviatoric strain and $K_{i\,(\boldsymbol{\epsilon}_p,T)}$ and $G_{i\,(\boldsymbol{\epsilon}_p,T)}$ are the bulk and shear moduli, respectively, which depend upon the temperature and the plastic strain, through the following functions

$$K_{i\,(\boldsymbol{\epsilon}_p,T)} = \left[a_K - b_K \Delta T - c_K \tanh\left(\frac{T - T_K}{d_K T_0}\right)\right] \exp[-a_1 \mathrm{tr}\boldsymbol{\epsilon}_p] \exp[-a_2 \mathrm{tr}(\mathbf{e}_p \cdot \mathbf{e}_p)], \tag{50}$$

$$G_{i\,(\boldsymbol{\epsilon}_p,T)} = K_{i\,(\boldsymbol{\epsilon}_p,T)} \frac{2(1+\nu)}{3(1-2\nu)}, \tag{51}$$

in which a_K, b_K, c_K, d_K and T_K are constitutive parameters that have to be calibrated using experimental measurements and ν is the (assumed constant) Poisson's ratio. It is worth remarking that elasto-plastic coupling is introduced through the dependency of $K(T, \boldsymbol{\epsilon}_p)$ and $G(T, \boldsymbol{\epsilon}_p)$ on $\boldsymbol{\epsilon}_p$. Note that an increase of plastic deviatoric strain and plastic dilatation ($\mathrm{tr}\boldsymbol{\epsilon}_p > 0$) leads to a degradation of elastic stiffness, whereas a plastic compaction ($\mathrm{tr}\boldsymbol{\epsilon}_p < 0$) leads to an increase of elastic stiffness.

The functions $\alpha_{(T)}$ and $\tilde{c}_{p\,(T)}$ simulate the observed dependence on temperature of the thermal expansion coefficient and of the heat capacity, through the following relationships

$$\alpha_{(T)} = a_A + b_A \left(\frac{T - T_A}{T_0}\right)^{e_A}, \qquad \tilde{c}_{p\,(T)} = a_C + b_C \left(\frac{T - T_C}{T_0}\right)^{e_C}, \tag{52}$$

where a_A, b_A, e_A, T_A, a_C, b_C, and T_C are constitutive coefficients that have to be calibrated using experimental measurements. The function $\tilde{c}_{p\,(T)}$ is related to $\tilde{c}_{v\,(T)}$ in equation (31), through

$$\tilde{c}_{v\,(T)} = \tilde{c}_{p\,(T)} - \frac{1}{\rho} K_{i\,(\boldsymbol{\epsilon}_p,T)} \alpha^2_{(T)}. \tag{53}$$

Having assumed the laws (49)-(52), the evolution with temperature remains defined for the adiabatic and isothermal elastic moduli, for the linear thermal expansion coefficient, and for the specific heats at constant strain and at constant stress (the latter is

defined through the complementary elastic energy) which are reported in Fig. 1. Note that the values of heat capacity were obtained at constant atmospheric pressure (0.1 MPa), whereas the values of heat capacity at constant strain were evaluated for the current volume of the sample (which is subject to an increase of temperature). Even if a large variation of temperature is analysed, the specific heats at constant strain and at constant stress nearly coincide with each other (Fig. 1 upper part) and agree with the available data on sintered alumina.

3.2 Yield function and hardening laws

A simple example of the introduced general framework involving elasto-plastic coupling with a non-linear dependence of elastic properties on the temperature is now developed with reference to a temperature-dependent yield function assumed to be the following extension of the modified Cam Clay model

$$f(\boldsymbol{\sigma}, T, p_c) = M_{cv} K_{(\theta)} \left[\left(\frac{\mathrm{tr}\boldsymbol{\sigma}}{3} - \tilde{p}_t \right)^2 + \left(\frac{\mathrm{tr}\boldsymbol{\sigma}}{3} - \tilde{p}_t \right) (\tilde{p}_c + \tilde{p}_t) \right] + 3J_2, \tag{54}$$

where M_{cv} is the critical state slope parameter, $K_{(\theta)}$ is a function of the Lode angle, θ, describing the deviatoric section (assumed in the form proposed in [1]), J_2 is the second deviatoric stress invariant, $\tilde{p}_c = p_c R_{(T)}$ is the yield stress under isotropic compression (function of the temperature through $R_{(T)}$), p_c is the hardening parameter (denoted by $\mathcal{H}$ in equation (18)), representing the compaction pressure and depending on the plastic volumetric strain through the Cooper and Eaton [7] relation

$$\mathrm{tr}\boldsymbol{\epsilon}_p = -\tilde{a}_1 \mathrm{exp}\left(-\frac{\Lambda_1}{p_c} \right) - \tilde{a}_2 \mathrm{exp}\left(-\frac{\Lambda_2}{p_c} \right), \tag{55}$$

and $\tilde{p}_t = k\tilde{p}_c$ is the yield stress under isotropic extension, assumed to be a fraction k of the yield stress for isotropic compression. The scalar function $R_{(T)}$ of temperature in equation (54) is a thermal reduction factor describing the thermal softening of the yield surface occurring at high temperature, due to the partial melting of some constituents. $R_{(T)}$ is assumed in the following form

$$R_{(T)} = a_R + b_R \mathrm{tanh}\left(\frac{T - T_R}{c_R T_0} \right), \tag{56}$$

where a_R, b_R, c_R, and T_R are constitutive parameters to be calibrated using experimental results. At room temperature $R_{(T)} \leq 1$ is equal to the unit and decreases at large temperatures. Due to the lack of available experimental data, the evolution of $R_{(T)}$ with temperature is assumed similar to that governing the elastic stiffness (see Fig. 1 upper part) and is shown in Fig. 2.

Isotropic hardening is assumed to be described by $p_c R_{(T)}$, which depends on both the volumetric plastic strain (through p_c, which can induce either hardening or softening) and on the temperature (through $R_{(T)}$).

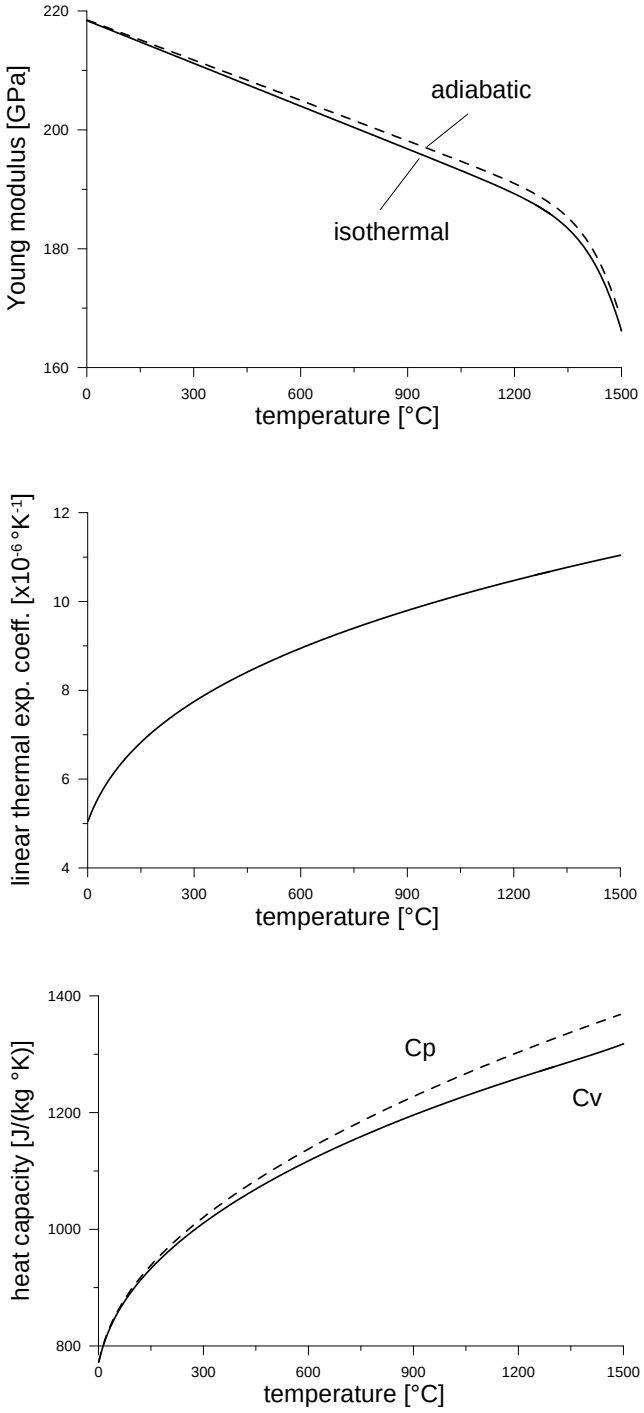

Figure 1: Laws describing the variation with temperature of: adiabatic and isothermal elastic modulus (upper part), linear thermal expansion coefficient (central part) and specific heats at constant strain and at constant stress (lower part), evaluated at atmosferic pressure.

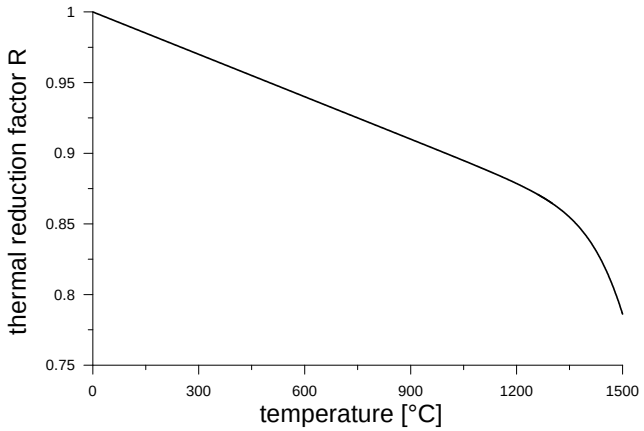

Figure 2: Law describing the variation of the thermal reduction factor $R(T)$ with temperature, describing thermal softening of the yield surface occurring at high temperatures.

4 Simulations of loading/unloading triaxial tests with temperature variations

The results of simulations of triaxial tests involving cyclic quasi-static loadings with temperature variations are presented in this Section. The results were obtained using the two sets of constitutive parameters provided in the Table 1. The calibration of the constitutive parameters given in Table 1 can be obtained from standard laboratory tests, measuring the dynamic elasticity moduli, the thermal expansion coefficient and the heat capacity at different temperature (at atmospheric pressure), and performing unconfined compression tests at various temperatures. The calibration of the temperature-dependent constitutive parameters employed in the present study and reported in Table 1 was obtained from the experimental data available from [9] and [28]. The simulations were obtained through integration of the constitutive equations in rate form via a fully-implicit backward Euler method at prescribed incremental strain, by enforcing a traction controlled boundary condition. The initial temperature is assumed equal to $T_o = 290^o$ K. An extreme variation of parameters was used to highlight peculiarities of the model behaviour. In particular, the effects of a thermal loading-unloading cycle were simulated assuming an elastic stiffness typical of dynamic measurements (and therefore high), whereas isotropic compression tests and triaxial compression tests were simulated assuming an elastic stiffness typical of static tests, and therefore low, so that it was taken to be 1/10 of the dynamic stiffness.

4.1 Simulation of an isotropic compression loading-unloading test performed at room temperature

Fig. 3 (upper part) shows the simulations of an isotropic compression loading-unloading test. The initial size of the yield stress is defined by the initial values $p_c = 30$ MPa and $R = 1$. The initial isotropic stress is equal to -10 MPa. As a result, elasto-plastic loading occurs between -30 and -40 MPa, as can be deduced from the change of slope in Fig. 3 (upper part) and from the irreversible strains upon unloading. Although not clearly appreciable in Fig. 3 (upper part), the loading and the unloading curves have a different slope. The variation of elastic stiffness is reported in Fig. 3 (lower part), as a function of the volumetric strain. It can be noted that the mechanically-driven plastic compaction induces, through elasto-plastic coupling, a relevant increase in elastic stiffness (from 21.8 to 25.5 GPa).

4.2 Simulation of a thermal cycle performed at a constant isotropic pressure

Figure 4 (upper part) shows the softening/hardening induced by a thermal cycle applied to a sample subject to a constant isotropic stress state equal to -40 MPa. The initial size of the yield stress is defined by $p_c = 45$ MPa and $R = 1$, so that the stress state initially lies inside the yield locus and the material displays an elastic behaviour.

Due to thermal softening (described by the thermal reduction factor $R_{(T)}$), the yield surface shrinks up to the point A (Fig. 4, upper part), where the stress state touches the yield surface. Then, from point A onward, any further increase in temperature leads to a plastic compaction which is necessary to counterbalance the thermal softening with plastic hardening. Therefore, plastic strains occur between points A and B, as can also be observed in Fig. 5, where the volumetric strain produced during a thermal cycle is reported as a function of the applied temperature.

Subsequently, starting from B the temperature is decreased, so that thermal hardening occurs (associated to $R_{(T)}$) and the stress state returns inside the yield surface, so that the response becomes elastic. Due to the plastic compaction induced by the thermal cycle (Fig. 5), at the end of the cycle at room temperature, an irreversible volumetric compression (of about 0.5 %) has been generated, which is associated with a non-negligible increase of elastic stiffness (from 220 GPa to 230 GPa), through elasto-plastic coupling (Fig. 4, central part), and with a variation of heat capacities (Fig. 4, lower part, where the heat capacity at constant stress, c_p, is obtained taking the second derivative of the complementary potential of ψ with respect to the temperature).

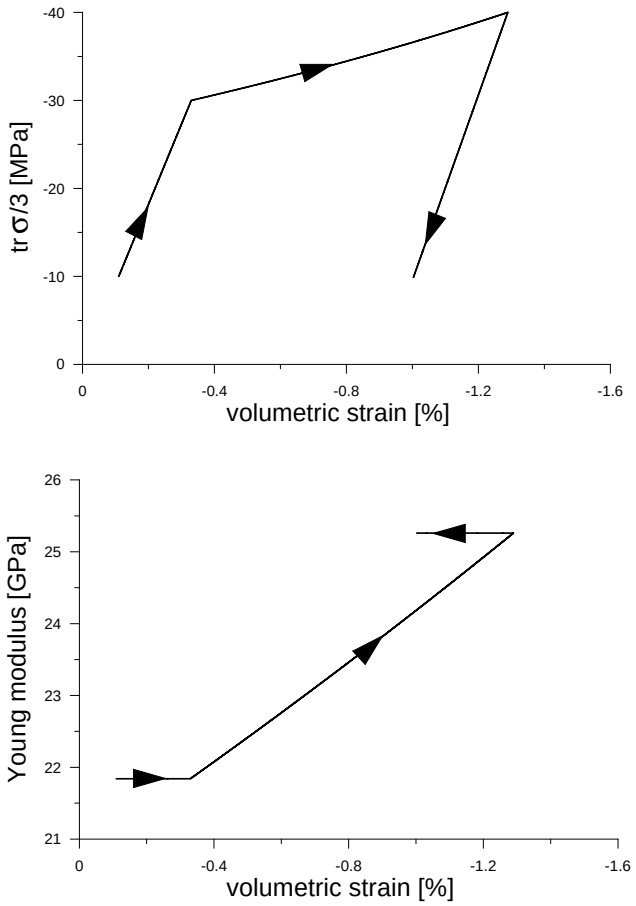

Figure 3: Simulation of an isotropic compression loading-unloading test at room temperature: mean stress versus volumetric strain (upper part) and variation of elastic modulus induced by plastic strain (lower part).

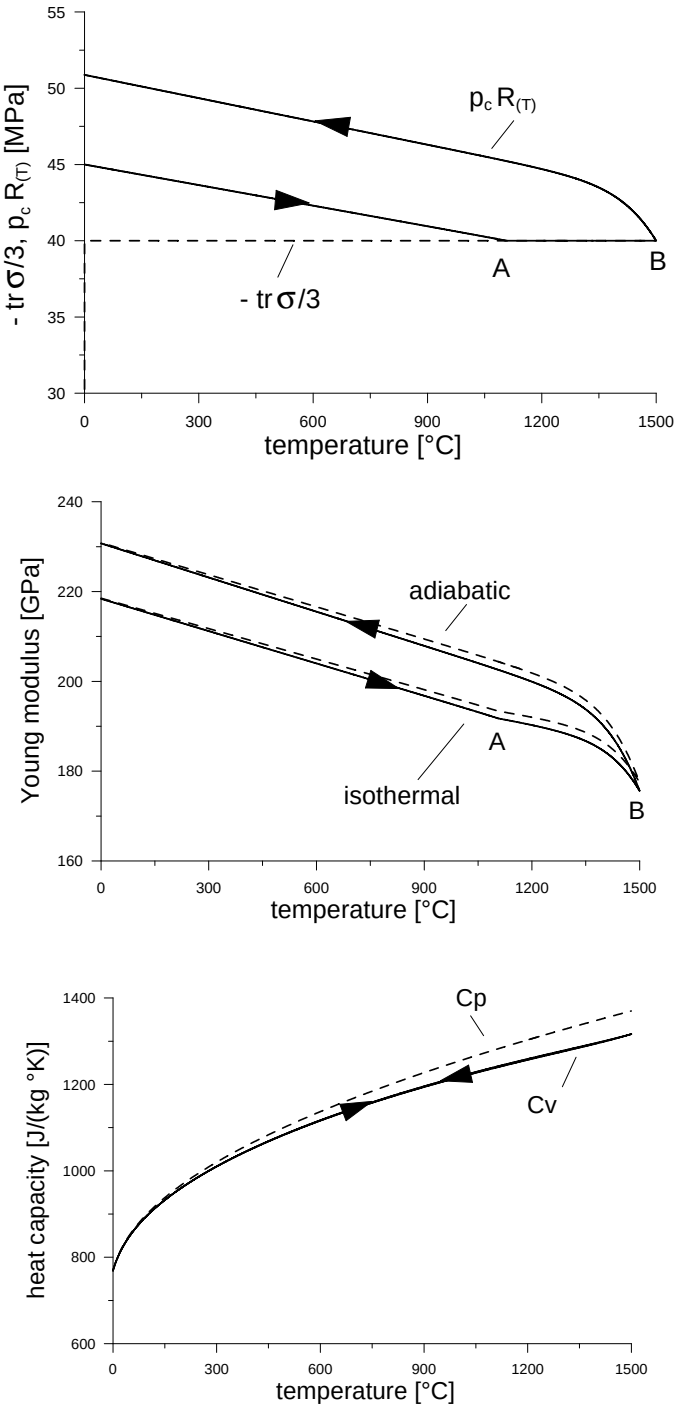

Figure 4: Simulated variation with temperature: of yield stress $p_c R_{(T)}$ of a sample subjected to a thermal cycle, at constant isotropic stress -40 MPa (upper part), adiabatic and isothermal elastic stiffness (central part), linear expansion coefficient and specific heats at constant strain and at constant stress (lower part).

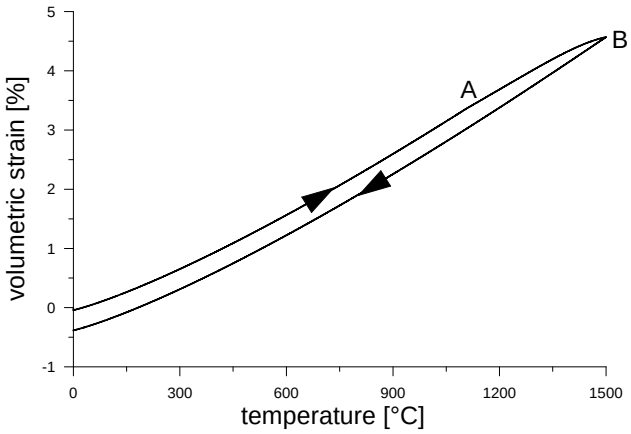

Figure 5: Simulated volumetric strain induced by a thermal cycle, at constant isotropic stress -40 MPa, versus temperature.

4.3 Simulation of a triaxial compression test with two unloading-reloading cycles at room temperature

In addition to the previously shown variation of the elastic stiffness associated with plastic compaction or swelling, the proposed thermo-elasto-plastic coupling constitutive framework also describes the degradation of elastic stiffness induced by deviatoric plastic strains, which are fundamental for the modelling of shear damage. This effect is quantified using the simulation of a triaxial compression test, performed on a cylindrical sample initially exposed to an isotropic stress equal to -1 MPa and later subject to increasing axial strain at constant radial stress. The initial size of the yield locus is defined by the values $p_c = 30$ MPa and $R = 1$. Fig. 6 shows the simulated axial stress (upper part) and volumetric strain (lower part) responses versus axial strain. After a peak strength is reached at a very small axial strain, the sample undergoes (homogeneous) softening and volumetric dilatancy. Note that strain localization is not considered in the results shown in Fig. 6. For a rigorous calculation with a full account of strain localization in a laboratory sample, the interested reader is addressed to Gajo and Bigoni [14]. Correspondingly, due to both the plastic deviatoric strain and the plastic volumetric dilatancy, a degradation of elastic stiffness occurs as a consequence of the elastoplastic coupling, which induces a marked decrease of elastic stiffness as can be observed from the elastic unload-reload cycles performed at different phases of shearing.

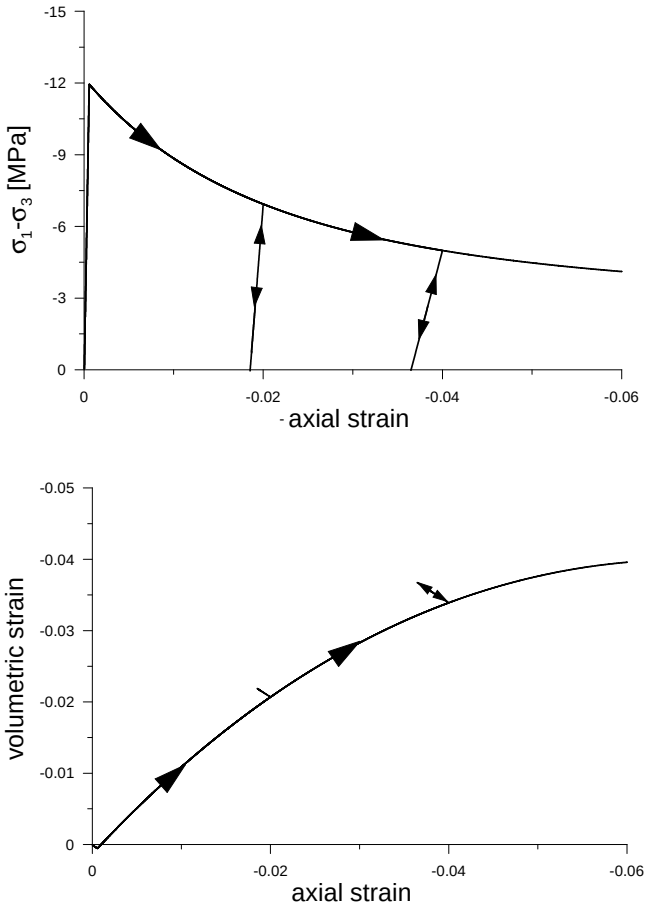

Figure 6: Simulation of a triaxial compression test at room temperature, involving two unloading-reloading cycles: deviatoric stress versus axial strain (upper part) and volumetric strain versus axial strain (lower part). Note that unloadings are reported evidencing elastoplastic coupling

5 Conclusions

Thermo-elasto-plastic coupling is a constitutive framework in which temperature influences both plastic flow and elastic stiffness of the material, but, independently of temperature, the former also influences the latter. For materials such as refractories, concrete, and rocks, this 'cross coupling' between temperature, plastic flow and elasticity is related to the fact that plastic flow is a macroscopic effect generated by the development of the collective response of a series of microdamage sources (pore collapse, sliding between grains, for instance), so that it influences the elastic response (which is sensitive to the amount of microdamage). Although temperature may accelerate microdamage it may also produce a self-healing effect through the melting of some constituents.

Thermo-elasto-plastic coupling has been derived with two procedures, one involving isothermal and the other involving adiabatic elastic moduli. The influence of temperature and plastic flow on the elastic stiffness has been clearly separated and commented. A final example of the application to sintered alumina has shown the capabilities of this model to describe the behaviour of refractories at high temperature or of sintering of ceramic powders.

Acknowledgements Financial support form the EU research project PIAPP-GA-2013-609758-HOTBRICKS is gratefully acknowledged.

References

[1] Argyris, J.H., Faust, G., Szimmat, J., Warnake, P., Willam, K. (1974) Recent development in finite element analysis of prestressed concrete reactor vessels. Nuclear Engineering and Design 28, 42-75.

[2] Benallal, A. and Bigoni, D. (2004) Effects of temperature and thermo-mechanical couplings on material instabilities and strain localization of inelastic materials. J. Mech. Phys. Solids , 52, 725-753.

[3] Bigoni D. (2012) *Nonlinear Solid Mechanics - Bifurcation Theory and Material Instability*. Cambridge University Press, 2012, ISBN:9781107025417.

[4] Bigoni, D. and Hueckel, T. (1991) Uniqueness and localization II. Coupled elastoplasticity. Int. J. Solids Structures 28, 215-224.

[5] Capurso, M. (1979) Extremum theorems for the solution of the rate problem in elastic-plastic fracturing structures. *J. Struct. Mech.* 7, 411-434.

[6] Collins, I.F. and Houlsby, G.T. (1997) Application of thermomechanical principles to the modelling of geotechnical materials. Proc. Royal Soc. A-Math. Eng. Sc. 453, 1964, 1975-2001.

[7] Cooper, A.R. and Eaton, L.E. (1962) Compaction behavior of several ceramic powders. J. Am. Ceram. Soc. 45, 97101.

[8] Damhof, F. Brekelmans, W.A.M., Geers, M.G.D. (2011) Predictive FEM simulation of thermal shock damage in the refractory lining of steelmaking installations. J. Materials Proc. Technology 211, 20912105.

[9] De Faoite, D., Browne, D.J., Chang-Diaz, F.R., Stanton, K.T. (2012) A review of the processing, composition, and temperature-dependent mechanical and thermal properties of dielectric technical ceramics. Journal of Materials Science 47 (10), 4211-4235.

[10] Galuppi, L. and Deseri, L. (2014) Combined effects of interstitial and Laplace pressure in hot isostatic pressing of cylindrical specimens. J. Mech. Materials Structures 9, 51-86.

[11] Fischer, G.J, and Paterson, M.S. (1989) Dilatancy during rock deformation at high temperatures and pressures. J. Geoph. Res., 94, B12, 17607-17617.

[12] Gajo, A. and Bigoni, D. (2008) A model for stress and plastic strain induced nonlinear hyperelastic anisotropy in soils. Int. J. Num. Anal. Meth. Geomech. 32, 833-861.

[13] Gajo, A. and Cecinato, F. (2015) Some considerations about selection of free-energy density function of refractory materials. In preparation.

[14] Gajo, A., Bigoni, D. and Muir Wood, D. (2004) Multiple shear band development and related instabilities in granular materials. J. Mech. Phys. Solids 52, 2683-2724.

[15] Gajo, A., Muir Wood, D. and Bigoni, D. (2007) On certain critical material and testing characteristics affecting shear band development in sand. Géotechnique 57, 449-461.

[16] Hueckel, T., (1975) On plastic flow of granular and rock-like materials with variable elasticity moduli. *Bull. Pol. Acad. Sci.*, Ser. Techn. 23, 405-414.

[17] Hueckel, T. (1976) Coupling of elastic and plastic deformation of bulk solids. *Meccanica* 11, 227-235.

[18] Hueckel, T. and Maier, G. (1977) Incremental boundary value problems in the presence of coupling of elastic and plastic deformations: a rock mechanics oriented theory. Int. J. Solids Structures 13, 1-15.

[19] Joliff, Y. Absi, J. Huger, M. and Glandus, J. (2008) Experimental and numerical study of the elastic modulus vs temperature of debonded model materials. Comp. Mat. Sc. 44, 826-831.

[20] Kodur, V. (2014) Properties of Concrete at Elevated Temperatures. ISRN Civil Engineering, Vol. 2014, Article ID 468510.

[21] Maier, G. and Hueckel, T. (1979) Non associated and coupled flow-rules of elastoplasticity for rock-like materials. *Int. J. Rock Mech. Min. Sci.* 16, 77-92.

[22] Olevsky, E., Molla, T.T., Frandsen, H.L., Bjork, R., Esposito, V. Ni, D.W., Ilyina, A., Pryds, N. (2013) Sintering of Multilayered Porous Structures: Part I-Constitutive Models. J. Am. Cer. Soc. 96, 2657-2665.

[23] Piccolroaz, A., Bigoni, D. and Gajo, A. (2006) An elastoplastic framework for granular materials becoming cohesive through mechanical densification. Part I - small strain formulation. Eur. J. Mechanics-A/Solids 25, 334-357.

[24] Piccolroaz, A., Bigoni, D. and Gajo, A. (2006) An elastoplastic framework for granular materials becoming cohesive through mechanical densification. Part II - the formulation of elastoplastic coupling at large strain. Eur. J. Mechanics-A/Solids 25, 358-369.

[25] Stupkiewicz, S., Piccolroaz, A. and Bigoni, D. (2015) Finite-strain formulation and FE implementation of a constitutive model for powder compaction. Comput. Meth. Appl. Mech. Engrg. 283, 856-880.

[26] Stupkiewicz, S., Denzer, R., Piccolroaz, A. and Bigoni, D. (2014) Implicit yield function formulation for granular and rock-like materials. Computational Mechanics 54, 1163-1173.

[27] Truesdell, C., Toupin, R.A. (1960) The classical field theories. In: Encyclopedia of Physics (Edited by S. Flügge) III/1, Springer-Verlag, Berlin.

[28] Werner, J., Aneziris, C.G., Dudczig, S. (2013) Young's Modulus of Elasticity of Carbon-Bonded Alumina Materials up to 1450 degrees C. Journal of the American Ceramic Society 96(9), 2958-2965.

[29] Ziegler, H. (1983) *A*n introduction to thermomechanics, 2nd edn. Amestardam: North-Holland.

Constitutive parameter		high stiffness	low stiffness
elastic stiffness	a_K [GPa]	73	7.3
	b_K [GPa/^{o}K]	1×10^{-4}	1×10^{-5}
	c_K [GPa]	18	1.8
	d_K	0.50	
	T_K [^{o}K]	1900	
	v	0.1	
thermal exp. coeff.	a_A	2×10^{-6}	
	b_A	5.5×10^{-6}	
	T_A [^{o}K]	250	
	e_A	0.3	
specific heat	a_C [J/m^3]	2.6×10^6	
	b_C [J/m^3]	8.8×10^5	
	T_C [^{o}K]	250	
	e_C	0.3	
elasto-plastic coupling	a_1	16	40
	a_2	8	20
yield surface	M_{cv}	1.07	
	k	0	
hardening functions	$\tilde{a}_1$	0.5	
	$\tilde{a}_2$	0.05	
	Λ_1 [GPa]	0.96×10^{-3}	
	Λ_2 [GPa]	0.41×10^{-1}	
	a_R	0.83	
	b_R [1/^{o}K]	1×10^{-4}	
	c_R	0.50	
	T_R [^{o}K]	1900	

Table 1: Constitutive parameters for sintered alumina:calibration obtained from avaliable data [9] and [28]